Startling C Behavior in Mo-Free Steel Atom Probe Tomography Volumes.

William Mottay, Jeremy Landes, Alain Portavoce, Benjamin Klaes, Frédéric Danoix, Philippe Maugis, Pierre Stocker, Carine Perrin-Pellegrino, Khalid Hoummada

Startling C behavior in Mo-free steel atom probe tomography volumes

W. Mottay[a,*], J. Landes[a,b], A. Portavoce[a], B. Klaes[c], F. Danoix[c], P. Maugis[a], P. Stocker[d], C. Perrin-Pellegrino[a], K. Hoummada[a]

[a]Aix Marseille Université, CNRS, IM2NP, 13397 Marseille, France
[b]Framatome, Développement (DTID) et Ingénierie Mécanique (DTIM), 92084 Paris La Défense, France
[c]Normandie Université, INSA Rouen, CNRS, Groupe de Physique des Matériaux, 76000, Rouen, France
[d]Aix Marseille Université, CNRS, ICR, 13397 Marseille, France

* Corresponding author: william.mottay@im2np.fr

Abstract

Atom probe tomography (APT) is now routinely used to study solute atom segregation at crystalline defects in different materials. The present study reports unexpected observations concerning carbon (C) segregation at dislocations in APT volumes analyzed from two different industrial steel grades. APT analyses reveal that C segregation at dislocations could only be observed with Mo co-segregation. Indeed, Transmission Electron Microscopy (TEM) observations on APT tips and correlative TEM-APT analysis show that despite dislocations being present in the samples prior to APT analyses, C segregation was not observed in the absence of Mo segregation. Statistics on the distribution of C composition in the different APT volumes from Mo-free steels show important discrepancies, with 35% of the volumes exhibiting C content in solid solution five times higher than expected. It is concluded that APT measurements of both C segregation at dislocations and C content in solution in iron may be incorrect due to the possibility of dislocations leaving the APT samples when subjected to a high electric field before or during field-evaporation.

Highlights

- C segregation at dislocations was observed by APT only with Mo co-segregation
- TEM images show that dislocations are present in the tips prior to APT analyses
- C segregation detection by APT at dislocations in steels without Mo is challenging
- C solid solution content in steel measured by APT present important inconsistencies

Keywords

Atom probe tomography, segregation, dislocations, steel, carbon

1. Introduction

Atom probe tomography (APT) is an advanced microscopy technique that offers unprecedented insights into the nanoscale structure and composition of materials (Baptiste Gault et al., 2012; Larson et al., 2013; Cerezo et al., 2007; Gault et al., 2021). By providing three-dimensional atomic-scale information, APT is a particularly useful tool for revealing local enrichments of solute atoms, especially in the context of segregation at crystalline defects such as dislocations (Blavette et al., 1999; Wilde et al., 2000; Takahashi et al., 2016; Zhou et al., 2021; Aboulfadl et al., 2015), grain boundaries (Zhou et al., 2016; Takahashi et al., 2012; Resende et al., 2021; Herbig et al., 2014), or the analysis of precipitates (Zandbergen et al., 2015; Takahashi et al., 2020; Kamboj et al., 2023; Landes et al., 2025), as to better understand the microstructure-properties relationship.

Regarding steels, it is well known that C segregates at dislocations, affecting their mechanical properties (Elsen & Hougardy, 1993; Pereloma & Timokhina, 2017; Lavaire, 2001; Belotteau, 2009; Marais, 2012; Baird, 1963; D V Wilson & Russell, 1960; D.V. Wilson & Russell, 1960; Da Rosa et al., 2017; Medouni, 2022; Medouni et al., 2021). C segregation is explained by the stress field existing around a dislocation (Hirth & Lothe, 1982; Friedel, 2013), which can be partially relieved by the accumulation of interstitial atoms in the surrounding of the dislocation, such as C and N in steels (Cottrell & Bilby, 1949; Veiga et al., 2013, 2015; Pascuet et al., 2017; Ventelon et al., 2023; Lüthi et al., 2018; Clouet et al., 2008; Cochardt & Schoek, 1955). Thus, C segregation at dislocations leads to a decrease of the system Gibbs free energy. Although a great deal of indirect evidence of C segregation at dislocations is available, it appears that C segregation at dislocations was not observed as often as expected in APT studies performed on steels.

An extensive literature review concerning C segregation at dislocations in steels using APT reveals surprising results. On the one hand, C segregation is observed in some steels (Miller, 2006; Smith et al., 2013; Liu & Zhao, 2012; Medouni, 2022; Medouni et al., 2021; Thuvander et al., 2021; Da Rosa et al., 2017; Macchi et al., 2024; Caballero et al., 2007; Xiao et al., 2016). On the other hand, some of the APT results available in the literature do not allow clear identification regarding the nature of local C enrichments (Pereloma & Timokhina, 2017; Park et al., 2010; Pereloma, Bata, et al., 2012; Soliman et al., 2020; Caballero et al., 2010; Pereloma, Beladi, et al., 2012). Without calling into question the relevance or the quality of the works cited above, some of these results raise questions about the real nature of the observed C enrichment: carbon segregated at a dislocation, carbon clusters, elongated carbide, APT artefact? The lack of published data on this specific issue, which has many industrial implications, is rather surprising.

In the present paper, solute atom segregation on dislocations is investigated by APT in two industrial steels used as structural materials for nuclear power plants: a low-alloy steel and a C-Mn steel. APT volumes were collected in both steels during two PhD theses, summing up to 156 volumes in the low-alloy steel and 171 volumes in the C-Mn steel. Dislocation density was estimated using transmission electron microscopy (TEM).

2. Materials and Methods

The first material is a low-alloy steel weld containing 0.095 C - 1.6 Mn - 0.9 Ni - 0.5 Mo - 0.25 Si - 0.007 N (wt%) (0.44 C – 1.63 Mn – 0.87 Ni – 0.3 Mo - 0.5 Si – 0.028 N in at %). The compositions were determined using optical emission spectroscopy or combustion analysis for C and N. Welding was carried out by deposition of 36 consecutive passes by submerged arc welding. The root and the skin of the weld were ground. The cooling time from 800 °C to 500 °C was estimated at 20 seconds for most welding passes. The microstructure of the weld metal is bainitic, which is consistent with that described in the literature (Jorge et al., 2021; Bhole et al., 2006). This first steel will be referred in this paper as the “0.5 Mo” steel.

The second material is a C-Mn steel weld containing 0.065 C - 1.37 Mn - 0.27 Si - 0.013 V - 0.014 N (wt%) (0.3 C – 1.38 Mn – 0.54 Si – 0.014 V – 0.056 N in at %). Welding was carried

out by deposition of 36 consecutive passes by manual arc welding. The cooling time from 800 °C to 500 °C was estimated at 5 seconds for most welding passes. The microstructure of the weld metal is a mix of acicular ferrite and polygonal ferrite, which is consistent with that described in the literature (Abson, 2018; Jorge et al., 2021). Previous studies on this weld exposed its sensibility to dynamic strain-aging (DSA), caused by C and N segregation at dislocations (Mottay et al., 2024). This steel will be referred in this paper as the "0 Mo" steel. The main difference between the two steels relies on the addition of Mo in the first one (as well as Ni, but it will prove unimportant for this study).

For both steels, a post-weld heat treatment (PWHT) was performed at 600°C for at least 90 minutes to relax internal stresses and reduce Dynamic Strain-Aging (DSA) sensitivity by precipitating C and N from solid solution into carbides and nitrides (Landes et al., 2025; Mottay et al., 2024; Wagner et al., 1996, 2000; Achar et al., 1998).

Dislocation density was estimated from TEM images with the line intercept method (Martin et al., 1995), using a microscope Tecnai from Thermo Fisher Scientific operated at 200 kV. APT analyses were performed on a Cameca LEAP 3000X-HR in voltage mode, with a 20% pulse fraction, 200 kHz pulse repetition rate and 0.5% detection rate. The specimen temperature was set at 50 K ("0 Mo" steel) or 65 K ("0.5 Mo" steel). The temperature has been optimized for both steels in order to maximize data quality without increasing the APT tips fracture rate. The detection efficiency of the equipment is 37%. APT data were reconstructed and treated using the IVAS 3.6.14 software. In these two steels, C composition measurements in voltage mode is not challenged by overlapping peaks with other elements, as might be the case for Ti-containing steels (Angseryd et al., 2011). C prominent peaks appear at 6 Da (C^{2+}), 12 Da (C^{1+}) and 24 Da (C_2^{1+}) in the mass spectra, without any overlap with other elements in this study. The possible presence of C_4^{2+} at 24 Da was not considered in this study, the reasons for it being discussed later. Typical mass spectra for both steels are presented in Supplementary Materials. APT tips and TEM foils were prepared in a dual-beam focused ion-beam and scanning electron microscope (FIB-SEM) Helios Nanolab 600 from Thermo Fisher Scientific, using the standard lift-out procedure (Larson et al., 2013), with two cleaning steps at 5 kV and 2 kV to limit Ga implantation.

3. Results

Figure 1 presents typical TEM images of the “0.5 Mo” (Fig. 1a) and the “0 Mo” steels (Fig. 1c). In the TEM images, the observed black lines are interpreted as dislocations. Indeed, dislocations disrupt the local crystalline order and affect electron diffraction. Diffraction contrast occurs when diffracted electrons interfere with transmitted electrons. This leads to bright and dark areas in the TEM micrographs, allowing dislocations to be visualized as black lines in bright field imaging mode (Hirth & Lothe, 1982; Saka, 2021). In both steels, the dislocation density was estimated to be 0.8-3 $\times$ 10^{14} m^{-2} using the line intercept method (Martin et al., 1995), on the basis of 10 TEM micrographs for each material. This value is in agreement with that reported in the literature for weld steels, about 10^{14} m^{-2}, with a possible under-estimation, less than a factor 2, of this value due to dislocation invisibility criterion (Yang & Bhadeshia, 1990; Mottay et al., 2024; Landes et al., 2025).

Typical APT samples are also presented for both the “0.5 Mo” steel (with Mo, fig. 1b) and the “0 Mo” steel (without Mo, fig. 1d). For “0.5 Mo”, solute atom local enrichments are observed along three lines, highlighted by 1 at % Mo iso-concentration surfaces in fig. 1b. Segregation of Mo, Mn and C are observed along these lines (fig. 2). According to the literature (Kamboj et al., 2023; Smith et al., 2013; Liu & Zhao, 2012; Medouni, 2022; Medouni et al., 2021), these local enrichments correspond to the segregation of the solute atoms along dislocations. It is worth noting that dislocations are observed only after PWHT in this material. No dislocations were observed in the as-welded condition.

A typical APT sample from the “0 Mo” steel is presented in Figure 1d. In this volume, a planar enrichment of solute atoms is observed, accompanied by atomic density variations along the same plane (fig. 2d). This is typical of C, Mn, and N grain boundary segregation (Takahashi et al., 2020; Langelier et al., 2017). Local enrichment of V and N atoms with a V/N ratio close to 1 is also observed, corresponding to a VN precipitate. The shape of the precipitate in the reconstructed APT data may be altered due to evaporation artefacts (Larson et al., 2013; B. Gault, Moody, et al., 2012). Cementite particles (Fe_3C) were observed in some APT volumes (not presented). Surprisingly, dislocations have not been observed in the “0 Mo” steel, with or without PWHT.

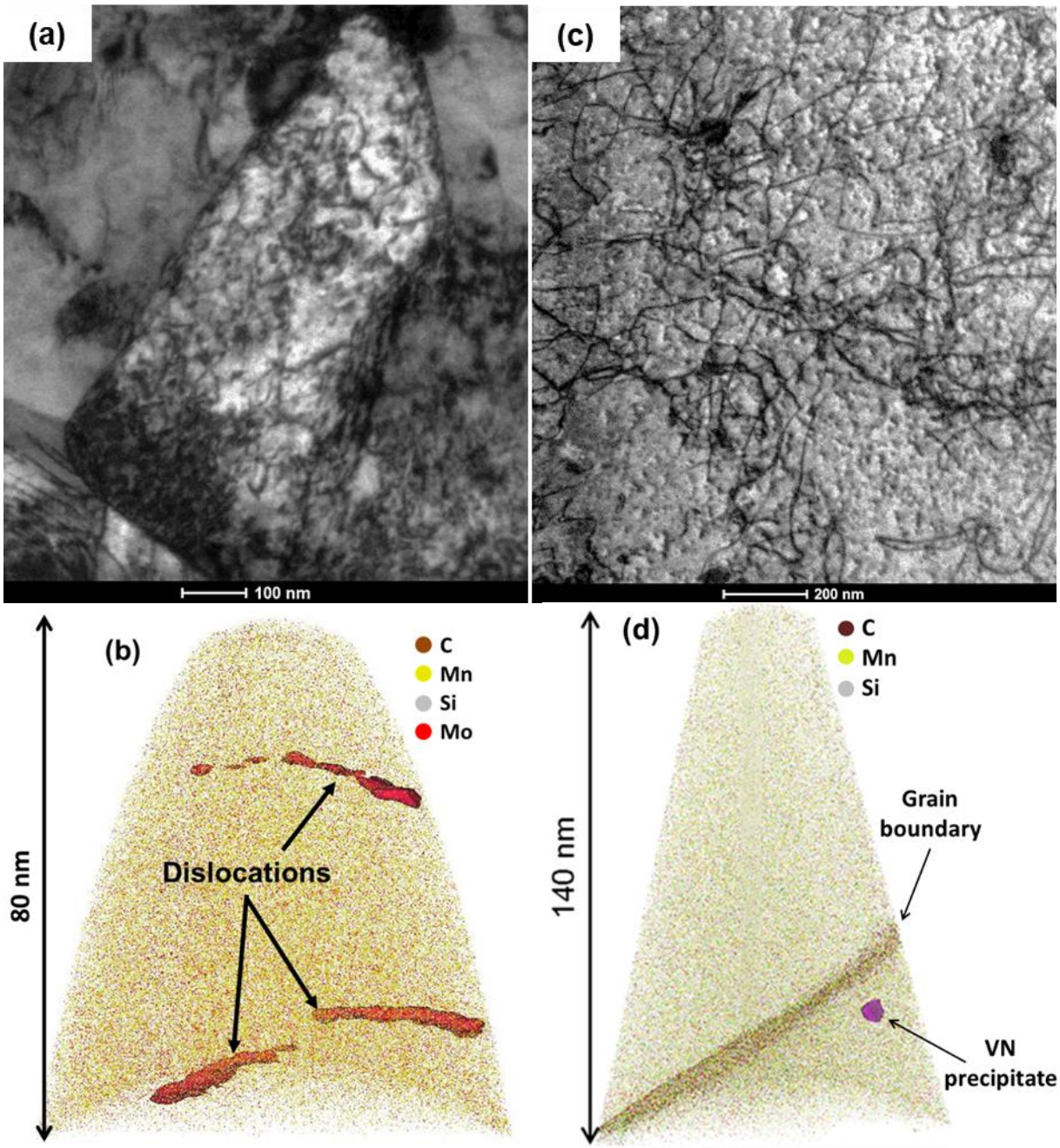

Figure 1: (a) typical bright-field TEM micrograph of the "0.5 Mo" steel, with a dislocation density estimated to 10^{14} m^{-2}.(b) typical APT sample from the "0.5 Mo" steel with segregation of solute atoms at dislocations highlighted by 1 at % Mo iso-concentration surfaces. (c) Typical TEM micrograph of the "0 Mo" steel, also exhibiting a dislocation density estimated to 10^{14} m^{-2}. (d) Typical APT sample from the "0 Mo" steel, showing a small precipitate and a decorated grain boundary. No decorated dislocation was observed in this material.

Solute enrichments on the different crystalline defects in the APT samples from fig. 1 are quantified in fig. 2. 1D concentration profile through the dislocations (radial direction) of "0.5 Mo" steel are plotted in fig. 2a (top dislocation), fig. 2b (bottom right dislocation) and fig. 2c (bottom left dislocation). These graphs clearly evidence C, Mn and Mo segregation on

dislocations, whereas Cr and Ni do not segregate on dislocations in this material (or weakly, as in fig. 2b). The excess of solute atoms along dislocation lines were quantified using the radial integral profile method proposed by Da Rosa et al. (Da Rosa et al., 2017). The excess of solute atoms on the top dislocation (fig. 2a) reaches 16 at.nm^{-1} for C, 11 at.nm^{-1} for Mn and 15 at.nm^{-1} for Mo. The excesses are 28 at.nm^{-1} (C), 12 at.nm^{-1} (Mn), 30 at.nm^{-1} (Mo), for the bottom right dislocation, fig. 2b, and 29 at.nm^{-1} (C), 7 at.nm^{-1} (Mn), 38 at.nm^{-1} (Mo) for the bottom left dislocation, fig. 2c. The 1D concentration profile across the grain boundary of "0 Mo" steel is presented in fig. 2d. It is seen that Mn, C and N segregate on the grain boundary with interfacial excess values (Maugis & Hoummada, 2016) being 3.5 at.nm^{-2} (Mn), 3.6 at.nm^{-2} (C) and 2.1 at.nm^{-2} (N).

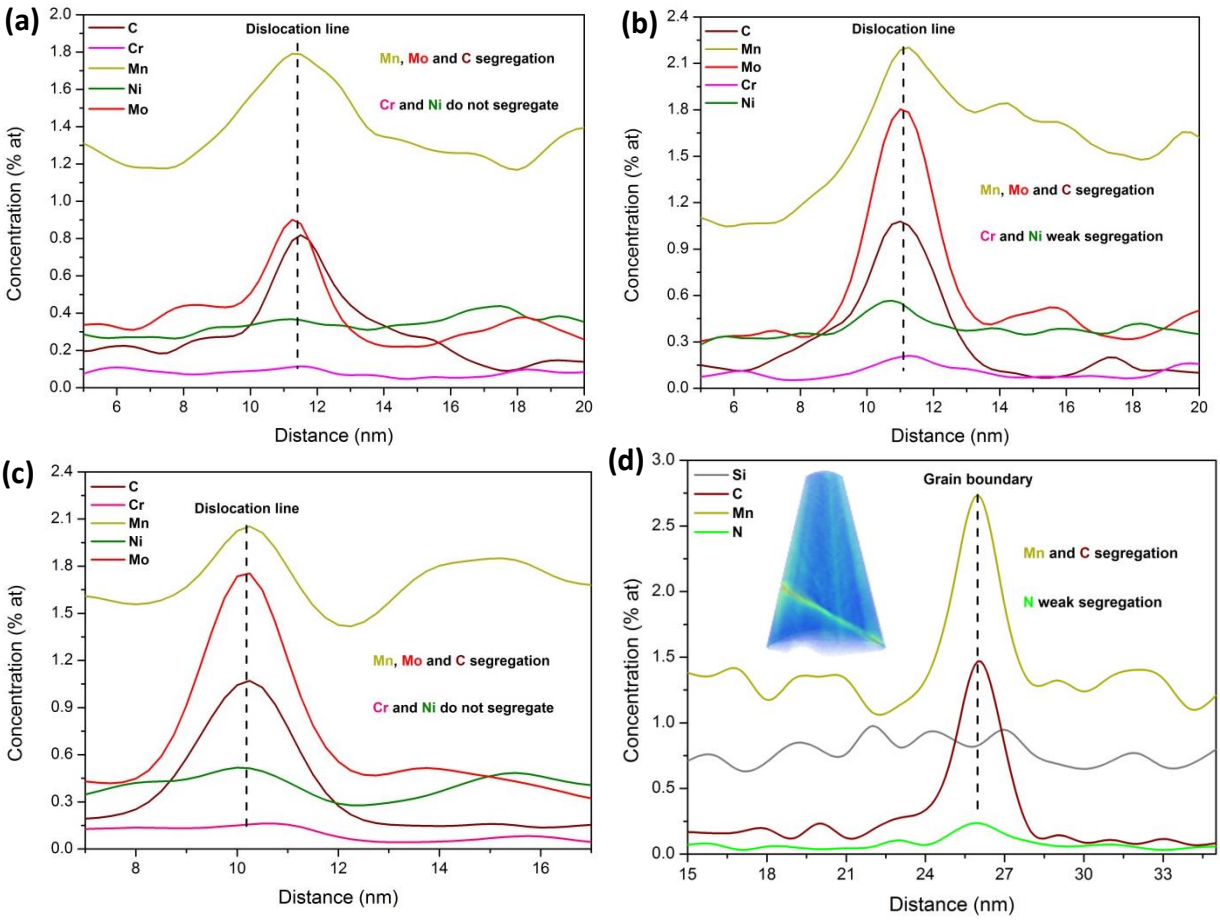

Figure 2 : Quantification of the different solute atom enrichments observed. (a-c) 1D concentration profile through the dislocations of "0.5 Mo" steel, in the radial direction (d) 1D concentration profile across the grain boundary from "0 Mo" steel. The Fe density map evidences a higher density of Fe ions at the grain boundary.

A 3D density map of iron in this APT sample is presented fig. 2d. Interestingly, it can be seen that there is a higher Fe density on the grain boundary. In other words, the grain boundary can be detected without the segregation of solute atoms, but only thanks to iron atoms. It

appears that dislocations observed in the “0.5 Mo” steel do not produce iron density variations (fig. 3).

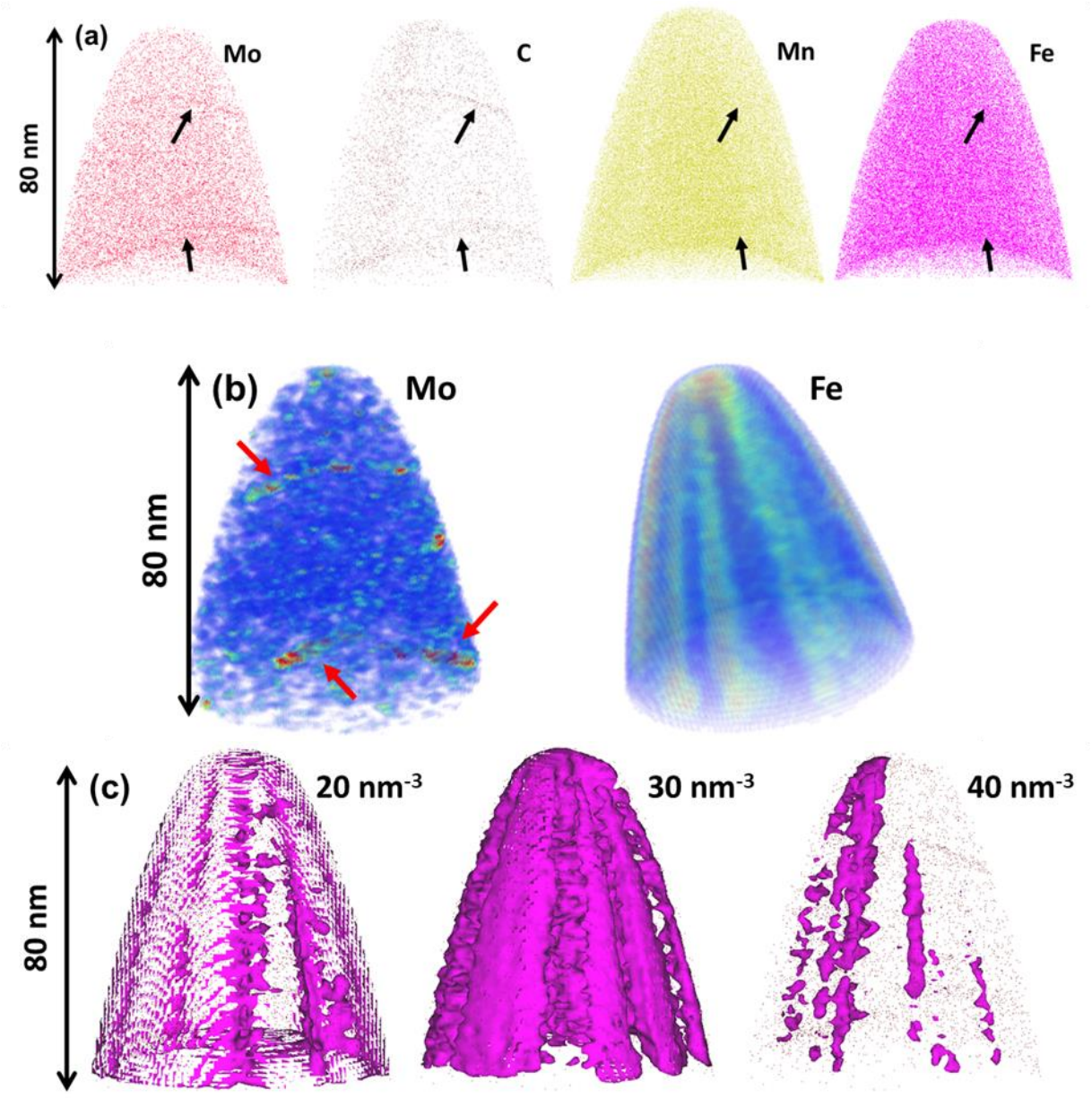

Figure 3 : Details of the dislocations observed in "0.5 Mo" steel (a) Mo, C and Fe atom maps. The dislocations are not observed in Fe atom map. (b) Heatmap of Mo and Fe atomic density in the volume. High densities are in red, low densities in blue. Dislocations are evidenced as high Mo densities but do not produce density variations of Fe. (c) Iso-densities of Fe at 20 nm^{-3} (low density), 30 $at.nm^{-3}$ (mean density) and 40 nm^{-3} (high density). Dislocations do not produce any density variations in Fe

Fig. 3 presents details of the APT volume from “0.5 Mo” steel (fig. 1b). Dislocations are observed from Mo and C atom maps (fig. 3a), arrowed in black. However, they are not distinguishable in Fe or Mn atom maps, where arrows point the expected location of dislocations. This has two major implications. First of all, Mn atoms do not allow the

dislocation to be located, even though they are segregated on the dislocation (≈ 10 at.nm^{-1}). This might be explained by the rather low Mn enrichment compared to the Mn content in the matrix. Moreover, dislocations do not produce Fe density variations in the APT samples. This observation is confirmed by further analyses of Mo and Fe density variations in the APT sample (fig. 3b) which reveal that dislocations appear as lines of higher Mo density but they do not produce Fe density variation. The absence of iron density variation is all the more confirmed in fig. 3c, which represents three iso-densities of Fe atoms: 20 at.nm^{-3} (low density), 30 at.nm^{-3} (about the mean density of Fe in the sample) and 40 at.nm^{-3} (high density). Then, it can be concluded that dislocations do not produce any density variations in iron, whether higher or lower densities. The reasons and consequences of these observations will be discussed later.

Previous research showed that FIB preparation, as well as some experimental techniques as TKD, could induce structural defects in the analyzed APT tips (Saksena et al., 2024; Tweddle et al., 2022; Gault et al., 2023). Based on these results, it could then be proposed that FIB-milling prevents the detection of segregation on dislocations. To investigate this hypothesis, the Ga implantation in the APT tips is presented for both the “0.5 Mo”, fig. 4a, and the “0 Mo”, fig. 4b. The “0.5 Mo” volume contains a dislocation, highlighted by a carbon iso-concentration with a threshold at 1 % at. C, Mo, Mn and N are segregated on this dislocation, with excess quantities of 6, 14, 4 and 3 at.nm^{-1}, respectively. Each blue dot represents a Ga atom, implanted during FIB preparation. The Ga content is equal to 0.005 at %, with a homogeneous distribution. The “0 Mo” volume contains small enrichment of vanadium, evidenced by V iso-concentration of 0.6 at %. These aligned precipitates are interpreted as VN particles, generally found on dislocations. Carbon does not enrich the precipitates and does not form a line joining the VN particles. However, the total carbon content in this “0 Mo” tip is 0.102 at %. A slight Ga enrichment is observed at the apex of the tip, because of FIB preparation, and the total Ga content is 0.017 at %. No Ga enrichment is found near the VN particles. Thus, a slight Ga implantation is observed in both the APT tips, because of FIB preparation. However, this contamination is extremely low, and not localized around atomic enrichments (precipitates, dislocations). Then, it is not expected that it could lead to C “desegregation”. Moreover, dislocations are observed in the “0.5 Mo” steel, which tips are prepared by FIB using the same procedure.

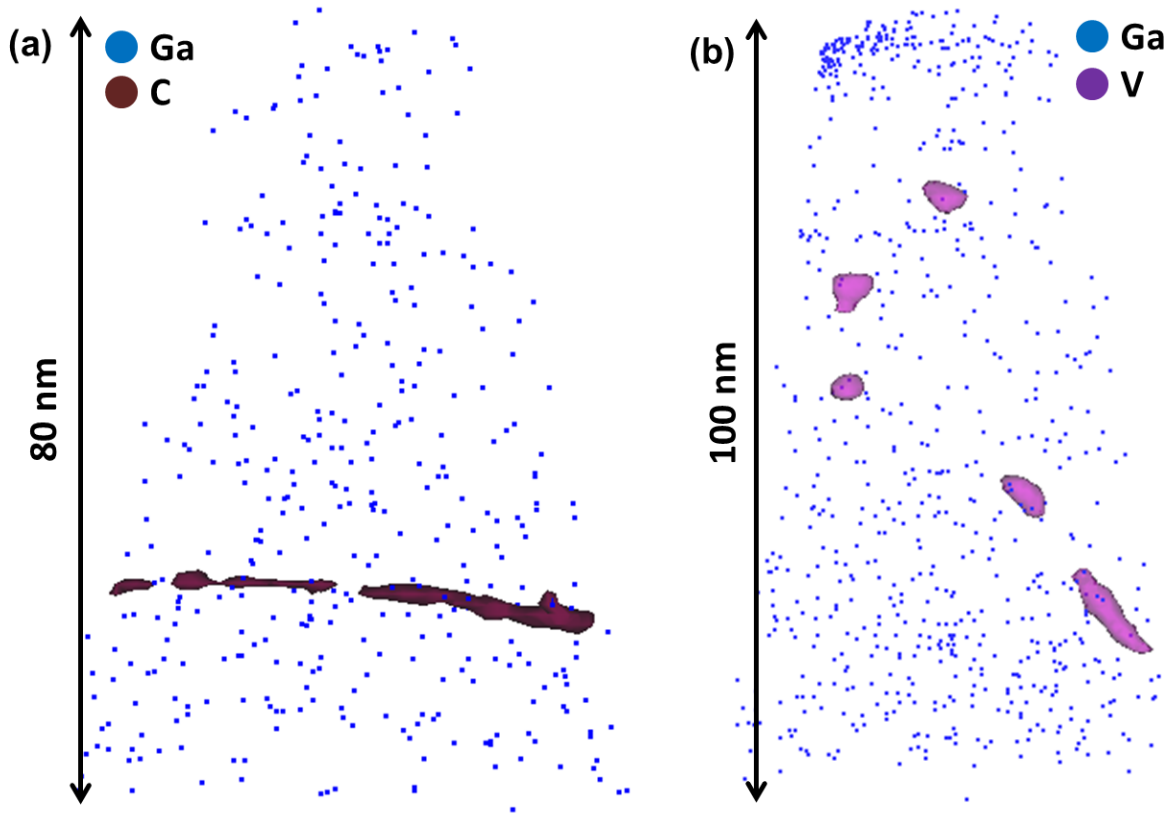

Figure 4 : Ga implantation in APT tips from (a) "0.5" Mo steel and (b) "0 Mo" steel. A slight Ga contamination is observed, but it is not localized around atomic enrichments. Dislocations are still observed in the "0.5 Mo" steel, even with Ga implantation due to FIB preparation.

The effect of preparation and analysis condition was further investigated in both steels, fig. 5. APT tips were prepared using the electropolishing method, in the "0.5 Mo" steel without heat-treatment, i.e. in a condition where dislocations are not observed. Fig. 5a presents a typical volume prepared by this method. An important carbon enrichment is identified, along with manganese and molybdenum, most probably corresponding to a cementite particle. The proxigram between the ferritic matrix and the precipitate is plotted, with the interface defined as a 12.5% carbon iso-concentration. This evidences that the carbon content in the precipitate is close to 25%, with an enrichment in manganese and molybdenum, suggesting that the precipitate is indeed a cementite particle, M_3C. However, dislocations were still not observed in tips prepared by the electropolishing method.

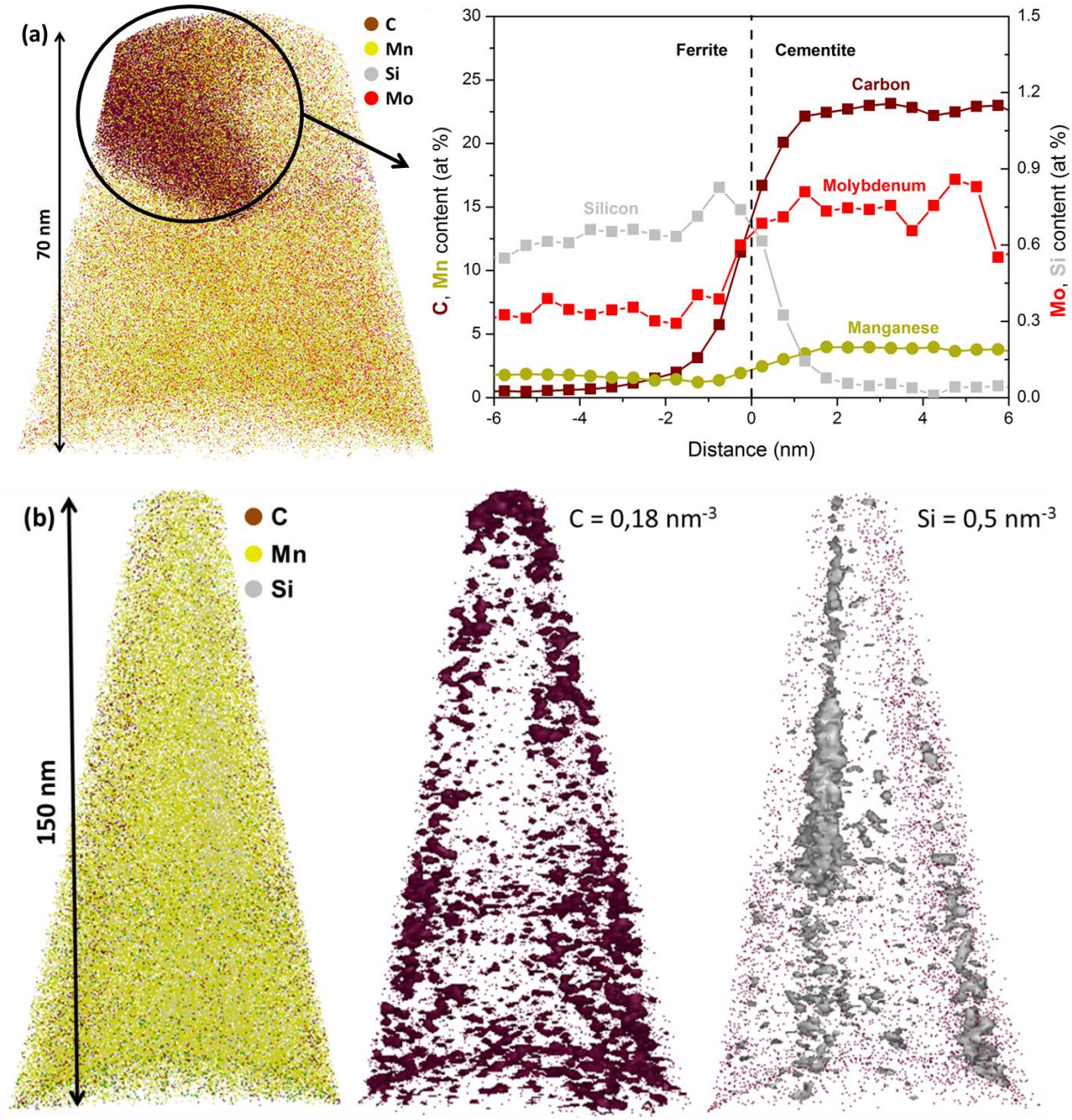

Figure 5 : (a) APT tip from "0.5 Mo" steel prepared by electropolishing method. (b) APT tip from "0 Mo" steel analyzed by laser pulsing

Furthermore, APT analyses were performed in the “0 Mo” steel in laser mode on a LEAP 6000 XR, at a base temperature of 50K, 200 kHz pulse rate and 30 pJ laser energy. Samples were FIB prepared. A typical volume, containing 12 million ions, is presented in fig. 5b. Some solutes, such as C and Si, present linear enrichment along the tip axis, or on the tip surface, evidenced by iso-densities of C (0,18 nm^{-3}) and Si (0,5 nm^{-3}). This results from surface migration of solute during APT analyses, as was already observed by Gault and collaborators (B. Gault, Danoix, et al., 2012), and is thus an APT artifact. The carbon content in this tip is rather high, reaching 0.052 at %, although no dislocation was observed. Then, it seems that

laser-pulsed APT experiments do not allow observing C segregation on dislocations in the studied C-Mn steel.

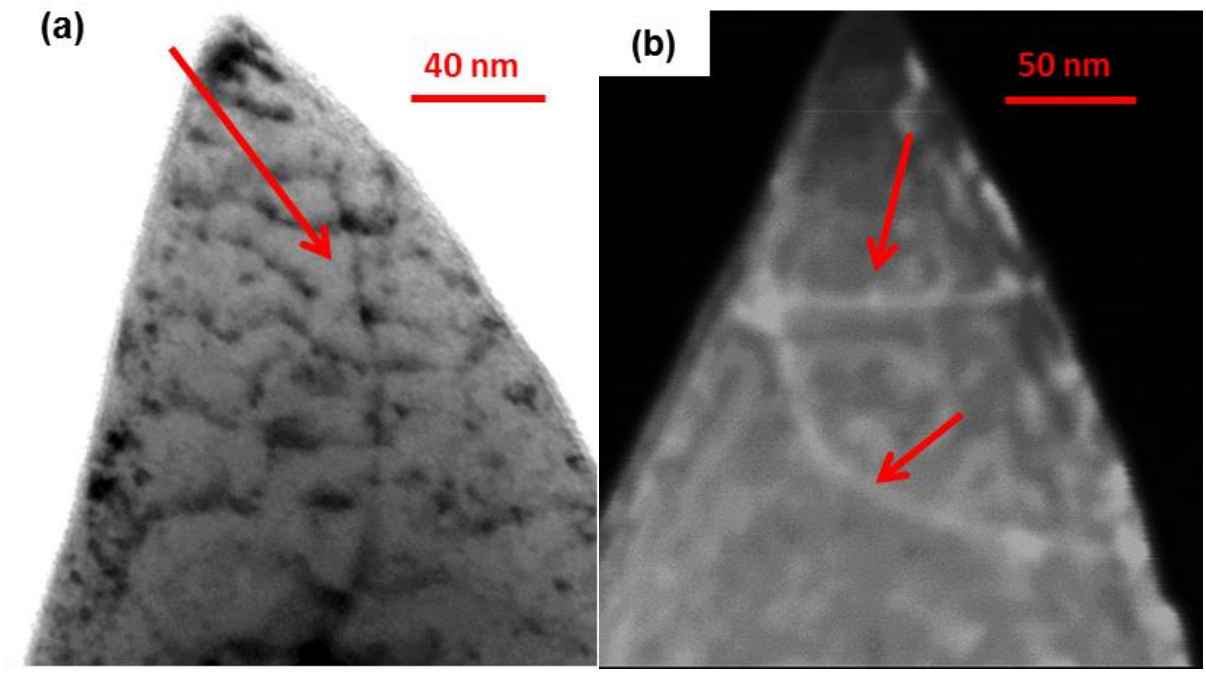

Figure 6 : Typical TEM images of the "0 Mo" steel tips prepared for APT measurements (a) bright-field and (b) dark-field condition. Dislocations (red arrows) are present in the samples after FIB preparation.

As was previously mentioned, in all the APT volumes analyzed from the "0 Mo" steel, not a single decorated region potentially corresponding to a dislocation could be observed. This is particularly surprising, as C is expected to segregate at dislocations. Indeed, the stress-strain curves from this material exhibit dynamic strain-aging sensitivity at 300 °C and elasto-plastic instabilities (yield point phenomenon) at 20 °C (Mottay et al., 2024). Both these phenomena are attributed to the interactions between C atoms and dislocations during plastic deformation (tensile tests at 300 °C) or prior to deformation, due to natural ageing (tensile tests at 20 °C). On average, APT samples collected in this steel contain 11 million ions, taking into account the 37% detection efficiency of the APT equipment. This leads to an average APT volume of 1.3×10^5 nm^3, based on the iron (Fe) atomic density of 84.7 $at.nm^{-3}$. The dislocation density in this sample being in the order of 10^{14} m^{-2}, a 40 nm long dislocation is expected to be observed every 3 APT samples. As previously mentioned, dislocations in Fe show no density variations in APT volumes, fig. 3 (contrasting with other crystalline defects such as grain boundaries, fig. 2d, or precipitates (B. Gault, Moody, et al., 2012; Zhou et al.,

2016)). Consequently, one cannot conclude whether the volumes are free of dislocation or C does not segregate at dislocations, thus preventing their observation.

TEM observations were performed on APT tips before field evaporation in order to investigate this lack of segregated dislocations in the APT samples. Fig. 6 presents TEM micrographs acquired on two different FIB-prepared APT tips from the “0 Mo” steel before evaporation. Dislocations are observed in the tips (red arrows) both in bright field (fig. 6a) or dark field (fig. 6b) conditions. Based on the dislocation density estimated from the TEM thin foils (Fig. 1), one dislocation should be observed for every 34 million atoms analyzed in APT, corresponding to one dislocation for every 3 analyzed APT samples. This is in relatively good agreement with the TEM observations performed on APT tips. Thus, dislocations are indeed present in some of the APT samples before analysis. Furthermore, the dislocations located in the APT tips should be present in the reconstructed volumes. For example, the dislocation in fig. 6a is located at about 40 nm from the tip apex. Therefore, it is expected to be observed in the corresponding APT volume. This result then suggests that the non-observation of segregation on dislocations in “0 Mo steel” is rather explained by a startling C behavior rather than by the absence of dislocations in the samples, at least before the APT analysis.

An in-depth study of APT volumes containing VN particles in the “0 Mo” steel reveals interesting results regarding C behavior. Indeed, VN particles tend to nucleate heterogeneously on dislocations (Gladman, 1997; Maugis & Gouné, 2005). Imaging of TEM thin foils reveals the presence of small precipitates (diameter < 5 nm), on dislocations (fig. 7a). Unfortunately, the small size of the precipitates did not allow for the identification of these particles, which are most probably small VN precipitates. Indeed, numerous VN precipitates were observed in APT volumes collected from the “0 Mo” sample, presented in fig. 7b (as well as in fig. 1d and 7c). On average, these precipitates contain 450 ± 100 atoms and are strictly vanadium nitrides, without carbon enrichment. Surprisingly, dislocations are not observed in these APT volumes, whereas VN are expected to precipitate on dislocations. Moreover, the C content in these APT volumes is abnormally high, 0.1 at % in fig. 7b and 0.062 at % on fig. 7c. This high C content cannot be explained by the presence of VN precipitates since they do not contain carbon.

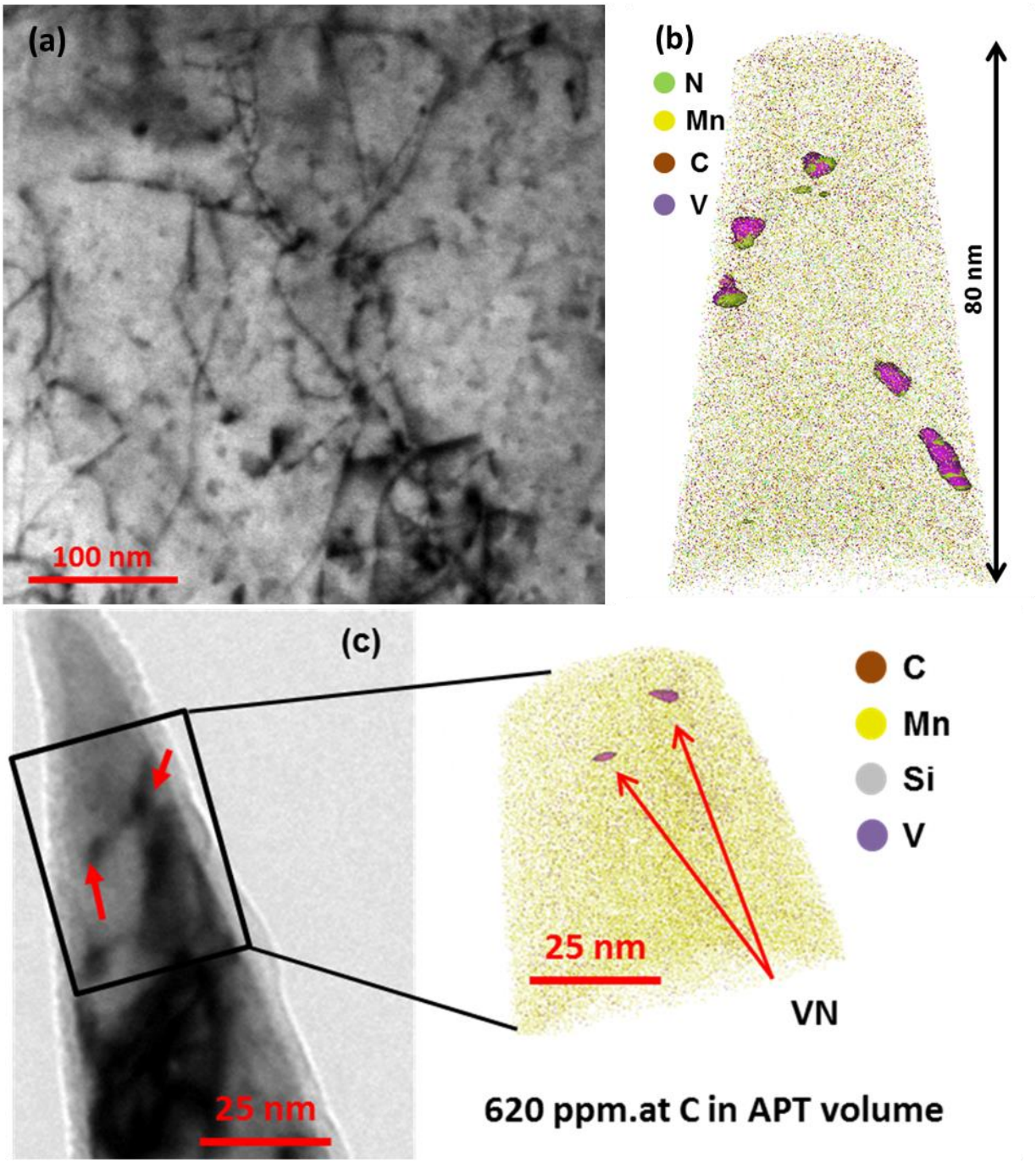

Figure 7 : (a) Typical TEM image from the "0 Mo" steel showing small precipitates (< 5 nm) on dislocations. (b) APT volume from the "0 Mo" steel evidencing small VN particles. No dislocation is observed in this volume. (c) Correlative TEM and APT analysis of a "0 Mo" tip. Two precipitates are visible in both TEM and APT (red arrows), evidence by 1 at % V iso-concentration. The dislocation linking the two precipitates in the TEM image is not observed in the APT volume

Fig. 7c presents the result of a correlative TEM-APT analysis performed on the "0 Mo" steel. An APT sample was prepared by FIB and observed in TEM, before being analyzed by APT. The TEM image reveals the presence of 2 small precipitates (red arrows) connected by a dislocation. These precipitates (VN particles) are indeed observed in the corresponding APT

volume. However, no linear solute enrichment connecting the two precipitates is observed in the APT volume, which could correspond to the dislocation observed in the TEM micrograph. Again, it is difficult to state if the dislocation moved during APT measurements (move toward the tip surface during field-effect evaporation for instance) or if it is not observed because C surprisingly does not segregate at the dislocation, despite a C content in this APT volume reaching 620 ppm.at and C room temperature diffusion (Gladman, 1997). Furthermore, as for the VN-containing APT volumes from fig. 7b, the C content in the APT samples appears abnormally high and cannot be explained by the presence of VN precipitates, which do not contain carbon. We have estimated the carbon concentration that could arise from the dislocation. We estimate the dislocation to be 30 nm long, with a mean carbon excess of 50 $at.nm^{-1}$. This leads to 1,500 carbon atoms on the dislocation. Considering that these atoms homogenize in the whole APT volume, which contains 4 million atoms, this leads to a carbon content of 0.0375 at %, to which we add the expected carbon content in the matrix, about 0.015 at %. This leads to a theoretical carbon content of 0.0525 at % in the APT volume, in close agreement with the measured value using APT, 0.062 at %.

It was shown that TEM imaging, and electron microscopy in general, could affect APT specimens by modifying carbon segregation on defects (Hickel et al., 2014; Tweddle et al., 2022; Saksena et al., 2024), and this might have happened in this correlative TEM-APT analysis (fig. 7c). However, the observed VN particles in APT samples are never on dislocations, and carbon content is excessively high, as is the case in fig. 7b. Besides, it was shown that cleaning steps at 5kV and 2kV during FIB preparation nearly hindered Ga contamination in the APT samples (Larson et al., 2013), as experimentally confirmed in fig. 4. Then, TEM observations from fig. 7c might have modified carbon segregation in the APT volume, but FIB preparation cannot explain the absence of C segregation on dislocations in all the other APT samples.

As mentioned previously, unexpected high C contents in solution in the “0 Mo” steel were found in a significant number of APT volumes. The distribution of C content in the different APT volumes of the “0 Mo” steel is presented in fig. 8a. The quantity represented on the y-axis corresponds to the number of APT volumes in a given class of carbon content, each multiplied by their ion quantity. This procedure limits the bias associated with the size of APT volumes. Larger volumes are given more weight than smaller ones. This statistical analysis

comprises only APT volumes analyzed in same conditions (50 K, 0.5% evaporation rate, 20% pulse fraction, and 200 kHz pulsing), exempt of C enrichment (such as grain boundary segregation or carbides), and with a minimum number of collected ions fixed at 2 million. Carbon compositions are background corrected. The same procedure is applied for the “0.5 Mo” steel (fig. 8b).

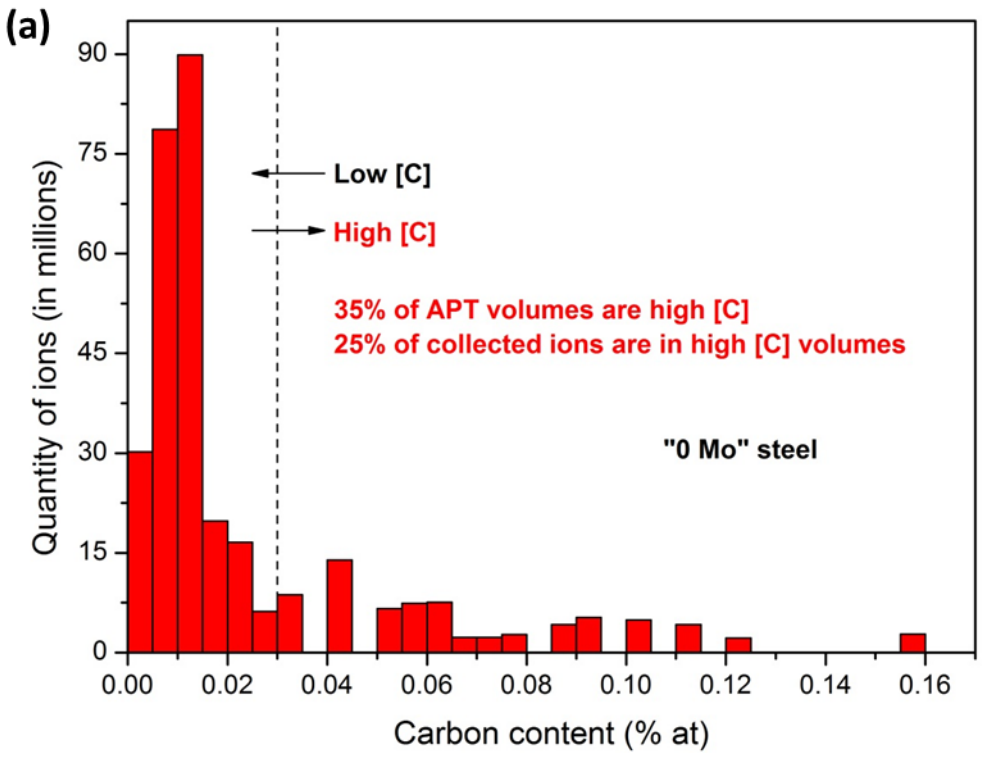

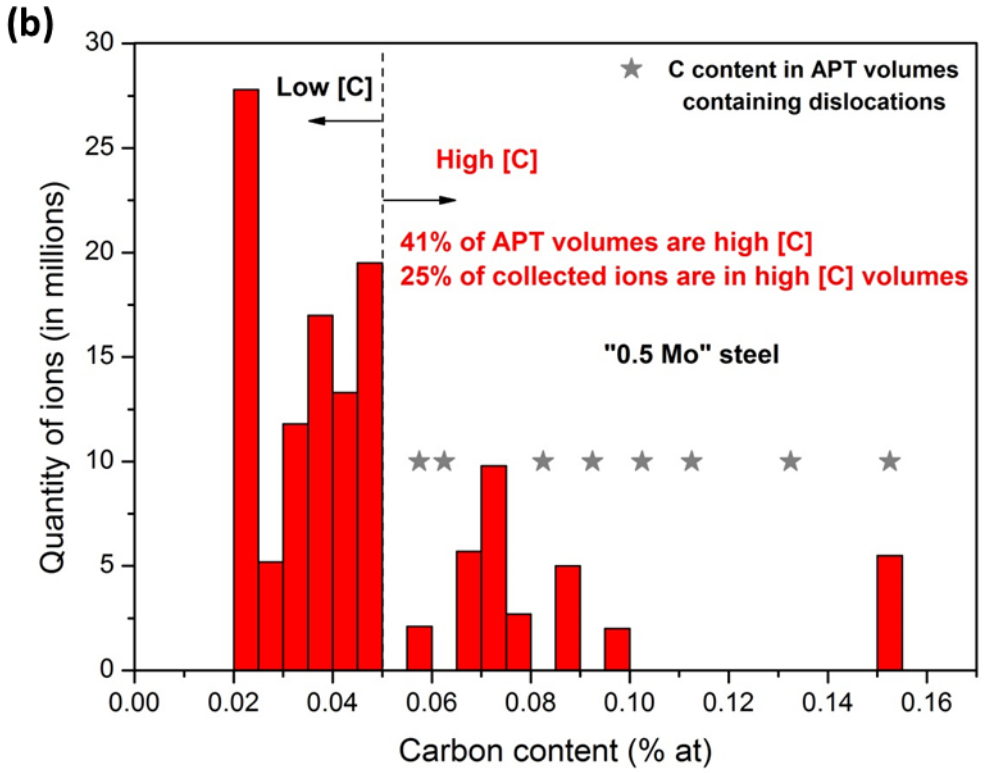

Figure 8 : Statistics on the C solution concentration measured in individual APT volumes from (a) "0 Mo" steel and (b) "0.5 Mo" steel. The "quantity of ions", y-axis, correspond to the number of APT volumes as a function of their carbon content, multiplied by the quantity of ions in each APT volume. Each material presents APT volumes with rather low carbon concentration (≤0.03 or 0.05 at %) as well as volumes with surprisingly high C content, which represent 35% of the volumes analyzed, or 25% of the ions collected. The carbon content of this volume is similar to the global carbon content of APT volumes in which dislocations were observed (grey stars).

As can be seen in fig. 8a, most of the APT volumes exhibit a C solution content close to 0.01 % at, in good agreement with the expected carbon composition in solid solution (considering that most of the carbon is precipitated as carbides (Wagner et al., 1996; Mottay et al., 2023; Wagner et al., 2000)). The distribution of these APT volumes follows a Gaussian-like distribution centered on 0.01-0.015 at %. Nevertheless, an important proportion of the APT volumes exhibits unexpected high C compositions in solution, reaching up to 0.16 at %. The threshold for these "high carbon" volumes is fixed at 0.03 at %, which seems to be the end on the Gaussian distribution. 35% of APT volumes, or 25% of the collected ions, present carbon content higher than 0.03 at %. Interestingly, this proportion of high carbon APT volumes (1 out of 3-4) is highly similar to the expected dislocation density (1 dislocation every 3 samples).

Statistics regarding C distributions were also performed on the “0.5 Mo” steel (fig. 8b). The same criterions were considered to include a sample in the analysis (identical APT analyses conditions, no C enrichment, 2 million ions minimum). The distribution of carbon content is rather peculiar. Once again, we consider two populations of carbon content. One with a carbon content smaller than 0.05 at %, which is considered as the solid solution (even though 0.05 at % is already a high value for C content in solid solution after post-weld heat treatment) and one with a carbon content larger than 0.05 at %, which is abnormally high and cannot be attributed to the solid solution. It was shown in fig. 1b that some dislocations are observed in the “0.5 Mo” steel. The carbon contents of these dislocations-containing samples are displayed as grey stars. The carbon value corresponds to the one of the whole volume, including the matrix and the segregation on the dislocations. It appears that the carbon content of these volumes containing a dislocation is similar to that measured in C-segregation-free volumes.

This suggests that the abnormally high C content comes from the segregation on dislocations that might have been homogenized. This proposition is all the more supported by the evidence that, as in the “0 Mo” steel, the high carbon volumes represent 41% of the APT samples, or 25% of the ions collected. In other words, the proportion of high carbon APT volumes is similar to the expected dislocation density, and the carbon content in these volumes is similar to the C content in dislocation-containing samples.

As was stated in the materials and methods section, the C prominent peaks appear at 6 Da (C^{2+}), 12 Da (C^{1+}) and 24 Da (C_2^{1+}) in the mass spectra, for both materials. It is well known that carbon is often detected as cluster ions that may overlap each other (i.e. C_2^{2+} and C^{1+} at 12 Da or C_2^{1+} and C_4^{2+} at 24 Da). In this study, C_2^{2+} and C_4^{2+} were not considered as possible cluster ions. Moreover, correlated field evaporation was demonstrated in the literature (Takahashi et al., 2011; Marceau et al., 2013), regarding the detection of carbon in steels. All these elements tend to minimize the detected carbon content and yields conservative results. In other words, the unexpectedly high carbon content cannot be explained by an overestimation of carbon in the mass spectra. However, it might be even higher if molecular carbon was indeed involved.

4. Discussion

Mo and C co-decorated dislocations are easily observed in APT volumes in Mo-containing steel samples (fig. 1b and 4a). Dislocation density is in agreement with that expected, as determined by electron microscopy. However, these segregated dislocations do not show density variations (fig. 3), suggesting that dislocations, in the studied steels, cannot be detected in APT volumes without sufficient impurity segregation (Mn segregates on dislocations, fig. 2, but cannot be used to locate the dislocations, fig. 3). In contrast, C segregated dislocations are not observed in APT volumes from samples free of Mo, despite the presence of dislocations in APT tips before field-evaporation (fig. 6 and fig. 7). Furthermore, the C content found in solution in the APT volumes can be significantly higher than expected. From these observations, the reason for dislocations not to be detected in APT volumes could be: i) C does not segregate at dislocations, despite its high content and room temperature ageing, ii) the dislocations are mobile during field-evaporation and leave the APT sample while segregated carbon atoms can homogenize in the volume, removing the trace of segregation, or iii) sample preparation modifies solute behavior.

APT sample preparation by FIB may possibly induce damages, resulting in a modified solute behavior (Saksena et al., 2024; Tweddle et al., 2022), but this cannot explain the absence of segregation on dislocations in the “0 Mo” steel as Ga implantation is limited in the first nanometers of the APT tips after a two steps cleaning procedure at 5 kV and 2 kV, as shown by Larson (Larson et al., 2013) and experimentally confirmed in fig. 4. Besides, samples from “0 Mo” and “0.5 Mo” steels were prepared using the same procedure on the same equipment. In both steels, a slight Ga contamination is observed, but dislocations are only observed in the “0.5 Mo steel”. The reason for that cannot be the specimen preparation, which is the same in both samples. C segregation could possibly be altered by FIB preparation, but it should be observed in both samples. Besides, electropolished tips, fig. 5a, did not reveal dislocations in the APT tips. This is in accordance with results available in the literature, where very few research evidence C segregation on dislocations in steels without Mo, whatever the preparation method. Supposing that electropolishing preparation allowed for detection and quantification of C segregation on dislocations in steels, it would be expected that much more results would have been published, as well as quantification of segregated C quantity in different conditions.

Concerning C segregation, further investigation in the as-welded “0.5 Mo” steel revealed that segregated dislocations are only detected in APT volumes after post weld heat-treatment (PWHT). Indeed, APT measurements performed on the as-welded “0.5 Mo” steel did not reveal any decorated dislocations out of 40 volumes. It is important to note that Mo atoms occupy substitutional Fe sites, while C atoms occupy interstitial sites. Consequently, the fact that Mo is not found to segregate at dislocations before PWHT can be explained by its low diffusion kinetics. However, C should be found at dislocations since its segregation is not kinetically limited. This observation leads to an important conclusion: APT measurements do not evidence C segregation, but evidence C and Mo co-segregation. Indeed, Mo-C attractive interactions are well known in steels (Thuvander et al., 2021; Gupta et al., 2022). Thus, three scenarios can be considered:

1) C does not segregate on dislocations without Mo;
2) Segregated Mo is able to prevent the displacement of dislocations during APT measurements, but not C. Then, C segregation is observed only with Mo, because Mo retains the dislocation in the sample;
3) Neither segregated C nor Mo can prevent dislocations to move and leave the APT sample during field-evaporation. However, Mo atoms are immobile at room temperature and mark the initial location of the dislocation the APT sample. The, due to Mo-C attractions, part of the segregated C atoms stay close to Mo, at the initial location of the dislocation.

The first scenario is not likely as C is known to segregate around dislocations (Cottrell & Bilby, 1949; Medouni et al., 2021; Veiga et al., 2013; Baird, 1971). One should note that in the last scenario, the amount of segregated C measured by APT might not correspond to the entire amount of segregated C, as interstitial C atoms located further away from Mo atoms (no Mo-C interaction) in the Cottrell atmosphere could leave after the desertion of the dislocation. This could explain the discrepancies observed between the segregated C amount measured experimentally by APT and theoretical expectations. Indeed, C dislocation segregation values reported by APT measurements are generally very low compared to calculated values (Veiga et al., 2013; Cochardt & Schoek, 1955).

Since atomic density variations in dislocation vicinity were never observed in iron APT volumes (fig. 3), even in the presence of Mo, the presence of the structural defect in APT volumes is not easily evidenced, allowing scenarios 2) and 3) to be considered. These scenarios are supported by our results obtained using correlative TEM-APT analyses and TEM images of APT tips, clearly showing the presence of dislocations in the tips prior to APT analysis (fig. 6). Correlative STEM-APT experiments were performed on a model Fe-9Mn alloy (Kuzmina et al., 2015; Kwiatkowski da Silva et al., 2017). Interestingly, the authors showed that all dislocations visible in STEM were not detected in APT due to a lack of solute segregation on some specific dislocations. Indeed, Mn, a substitutional atom in steels, is not expected to segregate around screw dislocations as they do not interact with substitutional atoms (Hirth & Lothe, 1982; Friedel, 2013). Then, the "invisible" dislocations in APT could be the screw ones. However, traces of carbon are present in the model Fe-9Mn, 0.035 at %, which are more than enough to induce a significant segregation on dislocations. The segregation of carbon on dislocations was not reported by the authors, whether because it was not the focus of their study, or whether because it was not detected by APT.

Besides, other defects, such as GBs and nano-clusters, show atomic density variations in iron APT volumes, as is the case in fig 2d. Finally, dislocations exhibit atomic density variations in other materials (Si, Ge (Perrin Toinin et al., 2016)). However, the ability of dislocations to move in APT tips at low temperature (20-80 K) during field-evaporation remains to be studied, even if the literature suggests that dislocations may be mobile when subjected to an electric field (Ba et al., 2020; Li et al., 2023, 2022; Huang, 2021; Birdseye & Smith, 1970; Rendulic & Müller, 1967), probably because of the induced stress. If dislocation motion in the APT tips during field evaporation is considered as possible, it most probably depends on the dislocation nature and its slip plane. Field Ion Microscopy (FIM) analyses, and more specifically 3D FIM analyses (Klaes et al., 2021) were performed on the "0 Mo" steel. These analyses did not evidence the presence of dislocations in the samples, suggesting that they were displaced by the applied electric field.

This study evidences the positive role of Mo on the detection of C segregation on dislocations. We suggest that other elements could have the same effect as Mo, provided that they respect some criterion:

1- They segregate on dislocations;
2- They have attractive interactions with carbon;
3- The ratio between the concentration on the defect and the bulk concentration is sufficient to identify the segregated element (Mn does not respect this criterion in this work, fig. 3)

We could expect Cr (Caillard, 2016) and B (Da Rosa et al., 2017) to have similar effects as Mo, in favoring the detection of C segregation on dislocations.

Furthermore, dislocation displacement towards the surface of APT tips during analysis could also explain the high C fraction measured in solution in some of the APT volumes. First, one can note that the statistic corresponding to APT volumes exhibiting an abnormally high C composition in solution matches that of APT volumes that should contain at least one dislocation (fig. 8). Second, APT volumes from the "0.5 Mo" steel containing C atoms co-segregated with Mo on a dislocation (fig. 8b) show a total amount of C similar to that found in the APT volumes from both steels showing unexpectedly high C content. For example, the APT volume from the "0.5 Mo" steel showed in fig. 1b contains a total of 730 at. ppm of C, while the APT volume from the "0 Mo" steel showed in fig. 7c contains a total of 620 at. ppm of C. These observations suggest that the high carbon APT volumes analyzed from the "0 Mo" steel were containing at least one dislocation with C segregation before APT measurements, but as the dislocations left the tip due to the applied electric field, C interstitial atoms could homogenize until no composition gradient could be found in the tip volume.

The mechanism for this homogenization is still unknown, but we could expect an effect of the applied electric field (B. Gault, Danoix, et al., 2012), or stress-induced diffusion during APT analysis (Birdseye & Smith, 1970; Rendulic & Müller, 1967). However, APT analyses using laser pulses do not enhance the detection of C segregation, compared to voltage pulses, fig. 5b. Then, it could also be proposed that the important surface-to-volume ratio of an APT tip leads to the diffusion of carbon to the free surface, rather than staying segregated on the dislocation line. The hypothetical diffusion of carbon to the free surface would be kinetically possible, considering the room temperature diffusion of carbon over a few tens of

nanometers, accelerated by pipe-diffusion. The apparent homogenization of carbon could be achieved due to carbon surface migration during the APT analysis, as evidenced in fig. 5b.

Conclusion

C segregation was studied by APT in two different steel welds containing similar dislocation densities, before and after post-weld heat treatment. The first steel contained Mo, while the second steel was Mo-free. TEM observations and correlative TEM-APT investigations were used to estimate the dislocation density in the two steels and to observe dislocations in APT tips. The results show that C segregation at dislocations could be detected only with Mo co-segregation, leaving no trace of dislocations in the APT volumes analyzed from the Mo-free steel. Furthermore, 35% of the APT volumes obtained from the Mo-free steel exhibit C content in solid solution unexpectedly high (up to five times the expected value). TEM observations confirmed that dislocations are present in some of the APT samples before field-evaporation, and APT measurements show no atomic density variations close to the dislocations revealed by C and Mo co-segregation.

These observations strongly suggest that dislocations have been “removed” from the APT volumes, possibly due to the high electric field applied to the samples in APT. In this case, Mo segregation could be still observed in APT volumes, even after the desertion of the structural defect, due to Mo (substitutional) very slow diffusion kinetics. The observed C co-segregation would result from the attractive interactions between these two elements. However, due to the short-distance Mo-C interactions, most of the segregated carbon is not paired to a Mo atom. This could explain the important differences between excess carbon atoms on dislocations experimentally determined using APT and the theoretical carbon excess on dislocations at equilibrium. In the Mo-free steel, the C atoms (interstitial) initially segregated at dislocations would be free to homogenize in the volume once the structural defect had deserted the sample, leading to homogenous C compositions and unexpected high contents.

Data availability

Data will be made available on request.

Acknowledgement

This project was supported by the National Association for Research and Technology, France (ANRT Project n◦ 2020/0883 and ANRT Project n° 2022/0152). This work was also supported by the European Union through the Program PIIEC ME/CT (project SCIRIUS, No. DOS0217953).

References

ABOULFADL, H., DEGES, J., CHOI, P. & RAABE, D. (2015). Dynamic strain aging studied at the atomic scale. *Acta Materialia* **86**, 34–42.

ABSON, D. J. (2018). Acicular ferrite and bainite in C–Mn and low-alloy steel arc weld metals. *Science and Technology of Welding and Joining* **23**, 635–648.

ACHAR, D. R. G., KOÇAK, M. & EVANS, G. M. (1998). Effect of nitrogen on toughness and strain age embrittlement of ferritic steel weld metal. *Science and Technology of Welding and Joining* **3**, 233–243.

ANGSERYD, J., LIU, F., ANDRÉN, H.-O., GERSTL, S. S. A. & THUVANDER, M. (2011). Quantitative APT analysis of Ti(C,N). *Ultramicroscopy* **111**, 609–614.

BA, X., ZHOU, M., ZHANG, X. & WANG, H. (2020). Manipulating Dislocations Using Electric Field to Repair Embrittlement Damage. *ISIJ International* **60**, 1803–1809.

BAIRD, J. D. (1963). *Strain Aging of Steel: a Critical Review*. Iron Steel.

BAIRD, J. D. (1971). The effects of strain-ageing due to interstitial solutes on the mechanical properties of metals. *Metallurgical Reviews* **16**, 1–18.

BELOTTEAU, J. (2009). 'Comportement et rupture d'un acier au C-Mn en présence de vieillissement sous déformation'. Ecole Centrale Paris https://tel.archives-ouvertes.fr/tel-01081269.

BHOLE, S. D., NEMADE, J. B., COLLINS, L. & LIU, C. (2006). Effect of nickel and molybdenum additions on weld metal toughness in a submerged arc welded HSLA line-pipe steel. *Journal of Materials Processing Technology* **173**, 92–100.

BIRDSEYE, P. J. & SMITH, D. A. (1970). The electric field and the stress on a field-ion specimen. *Surface Science* **23**, 198–210.

BLAVETTE, D., CADEL, E., FRACZKIEWICZ, A. & MENAND, A. (1999). Three-Dimensional Atomic-Scale Imaging of Impurity Segregation to Line Defects. *Science* **286**, 2317–2319.

CABALLERO, F. G., MILLER, M. K. & GARCIA-MATEO, C. (2010). Tracking solute atoms during bainite reaction in a nanocrystalline steel. *Materials Science and Technology* **26**, 889–898.

CABALLERO, F., MILLER, M., BABU, S. & GARCIAMATEO, C. (2007). Atomic scale observations of bainite transformation in a high carbon high silicon steel. *Acta Materialia* **55**, 381–390.

CAILLARD, D. (2016). Dynamic strain ageing in iron alloys: The shielding effect of carbon. *Acta Materialia* **112**, 273–284.

CEREZO, A., CLIFTON, P. H., GALTREY, M. J., HUMPHREYS, C. J., KELLY, T. F., LARSON, D. J., LOZANO-PEREZ, S., MARQUIS, E. A., OLIVER, R. A., SHA, G., THOMPSON, K., ZANDBERGEN, M. & ALVIS, R. L. (2007). Atom probe tomography today. *Materials Today* **10**, 36–42.

CLOUET, E., GARRUCHET, S., NGUYEN, H., PEREZ, M. & BECQUART, C. S. (2008). Dislocation interaction with C in α-Fe: A comparison between atomic simulations and elasticity theory. *Acta Materialia* **56**, 3450–3460.

COCHARDT, A. W. & SCHOEK, G. (1955). Interaction between dislocations and interstitial atoms in body-centered cubic metals. *Acta Metallurgica* **3**, 5.

COTTRELL, A. H. & BILBY, B. A. (1949). Dislocation Theory of Yielding and Strain Ageing of Iron. *Proceedings of the Physical Society. Section A* **62**, 49–62.

DA ROSA, G., MAUGIS, P., DRILLET, J., HEBERT, V. & HOUMMADA, K. (2017). Co-segregation of boron and carbon atoms at dislocations in steel. *Journal of Alloys and Compounds* **724**, 1143–1148.

ELSEN, P. & HOUGARDY, H. P. (1993). On the mechanism of bake-hardening. *Steel Research* **64**, 431–436.

FRIEDEL, J. (2013). *Dislocations: International Series of Monographs on Solid State Physics*. Smoluchowski, R. & Kurti, N. (Eds.). Amsterdam: Pergamon.

GAULT, B., CHIARAMONTI, A., COJOCARU-MIRÉDIN, O., STENDER, P., DUBOSQ, R., FREYSOLDT, C., MAKINENI, S. K., LI, T., MOODY, M. & CAIRNEY, J. M. (2021). Atom probe tomography. *Nature Reviews Methods Primers* **1**, 51.

GAULT, B., DANOIX, F., HOUMMADA, K., MANGELINCK, D. & LEITNER, H. (2012). Impact of directional walk on atom probe microanalysis. *Ultramicroscopy* **113**, 182–191.

GAULT, B., KHANCHANDANI, H., PRITHIV, T. S., ANTONOV, S. & BRITTON, T. B. (2023). Transmission Kikuchi Diffraction Mapping Induces Structural Damage in Atom Probe Specimens. *Microscopy and Microanalysis* **29**, 1026–1036.

GAULT, BAPTISTE, MOODY, M. P., CAIRNEY, J. M. & RINGER, S. P. (2012). *Atom Probe Microscopy*. New York, NY: Springer New York https://link.springer.com/10.1007/978-1-4614-3436-8 (Accessed September 20, 2023).

GAULT, B., MOODY, M. P., CAIRNEY, J. M. & RINGER, S. P. (2012). Atom probe crystallography. *Materials Today* **15**, 378–386.

GLADMAN, T. (1997). *The physical metallurgy of microalloyed steels*. 1. publ. London: Institute of Materials.

GUPTA, L., MAJI, B. C., NEOGY, S., SINGH, R. N. & KRISHNAN, M. (2022). Precipitation behaviour of 20MnMoNi55 RPV steel in the temperature range of 630–670 °C. *Materials Today Communications* **30**, 103096.

HERBIG, M., RAABE, D., LI, Y. J., CHOI, P., ZAEFFERER, S. & GOTO, S. (2014). Atomic-Scale Quantification of Grain Boundary Segregation in Nanocrystalline Material. *Physical Review Letters* **112**, 126103.

HICKEL, T., SANDLÖBES, S., MARCEAU, R. K. W., DICK, A., BLESKOV, I., NEUGEBAUER, J. & RAABE, D. (2014). Impact of nanodiffusion on the stacking fault energy in high-strength steels. *Acta Materialia* **75**, 147–155.

HIRTH, J. P. & LOTHE, J. (1982). *Theory of dislocations*. 2. ed. New York, NY: Wiley.

HUANG, Y. (2021). Electric features of dislocations and electric force between dislocations. *Mathematics and Mechanics of Solids* **26**, 616–628.

JORGE, J. C. F., SOUZA, L. F. G. DE, MENDES, M. C., BOTT, I. S., ARAÚJO, L. S., SANTOS, V. R. DOS, REBELLO, J. M. A. & EVANS, G. M. (2021). Microstructure characterization and its relationship with impact toughness of C–Mn and high strength low alloy steel weld metals – a review. *Journal of Materials Research and Technology* **10**, 471–501.

KAMBOJ, A., BACHHAV, M. N., DUBEY, M., ALMIRALL, N., YAMAMOTO, T., MARQUIS, E. A. & ODETTE, G. R. (2023). The effect of phosphorus on precipitation in irradiated reactor pressure vessel (RPV) steels. *Journal of Nuclear Materials* **585**, 154614.

KLAES, B., LARDÉ, R., DELAROCHE, F., HATZOGLOU, C., PARVIANIEN, S., HOUARD, J., DA COSTA, G., NORMAND, A., BRAULT, M., RADIGUET, B. & VURPILLOT, F. (2021). Development of Wide Field of View Three-Dimensional Field Ion Microscopy and High-Fidelity Reconstruction Algorithms to the Study of Defects in Nuclear Materials. *Microscopy and Microanalysis* **27**, 365–384.

KUZMINA, M., HERBIG, M., PONGE, D., SANDLÖBES, S. & RAABE, D. (2015). Linear complexions: Confined chemical and structural states at dislocations. *Science* **349**, 1080–1083.

KWIATKOWSKI DA SILVA, A., LEYSON, G., KUZMINA, M., PONGE, D., HERBIG, M., SANDLÖBES, S., GAULT, B., NEUGEBAUER, J. & RAABE, D. (2017). Confined chemical and structural states at dislocations in Fe-9wt%Mn steels: A correlative TEM-atom probe study combined with multiscale modelling. *Acta Materialia* **124**, 305–315.

LANDES, J., MOTTAY, W., HOUMMADA, K., PERRIN, C., MASSARDIER, V., JOUIAD, M., HERVE, N., MARCEAUX DIT CLEMENT, A. & MAUGIS, P. (2025). Precipitation of Manganese Nitride During Post-Weld Heat Treatment in C-Mn and Low-Alloy Steel Welds. *Metallurgical and Materials Transactions A*. https://link.springer.com/10.1007/s11661-025-07694-8 (Accessed February 4, 2025).

LANGELIER, B., VAN LANDEGHEM, H. P., BOTTON, G. A. & ZUROB, H. S. (2017). Interface Segregation and Nitrogen Measurement in Fe–Mn–N Steel by Atom Probe Tomography. *Microscopy and Microanalysis* **23**, 385–395.

LARSON, D. J., PROSA, T. J., ULFIG, R. M., GEISER, B. P. & KELLY, T. F. (2013). *Local Electrode Atom Probe Tomography: A User's Guide*. New York, NY: Springer New York https://link.springer.com/10.1007/978-1-4614-8721-0 (Accessed November 30, 2023).

LAVAIRE, N. (2001). 'Etude des phénomènes à l'origine du vieillissement des aciers pour emballage à Ultra Bas Carbone (ULC) : Apport du Pouvoir ThermoElectrique à la caractérisation des états microstructuraux'. INSA Lyon.

LI, M., SHEN, Y., LUO, K., AN, Q., GAO, P., XIAO, P. & ZOU, Y. (2023). Harnessing dislocation motion using an electric field. *Nature Materials* **22**, 958–963.

LI, X., TURNER, J., BUSTILLO, K. & MINOR, A. M. (2022). In situ transmission electron microscopy investigation of electroplasticity in single crystal nickel. *Acta Materialia* **223**, 117461.

LIU, Q. & ZHAO, S. (2012). Cu precipitation on dislocation and interface in quench-aged steel. *MRS Communications* **2**, 127–132.

LÜTHI, B., VENTELON, L., RODNEY, D. & WILLAIME, F. (2018). Attractive interaction between interstitial solutes and screw dislocations in bcc iron from first principles. *Computational Materials Science* **148**, 21–26.

MACCHI, J., TEIXEIRA, J., DANOIX, F., GEANDIER, G., DENIS, S., BONNET, F. & ALLAIN, S. Y. P. (2024). Impact of carbon segregation on transition carbides and cementite precipitation during tempering of low carbon steels: Experiments and modeling. *Acta Materialia* **272**, 119919.

MARAIS, A. (2012). 'Influence du vieillissement statique sur la transition ductile-fragile des aciers au C-Mn'. Paris: Ecole nationale supérieure des Mines de Paris https://www.theses.fr/2012ENMP0081.

MARCEAU, R. K. W., CHOI, P. & RAABE, D. (2013). Understanding the detection of carbon in austenitic high-Mn steel using atom probe tomography. *Ultramicroscopy* **132**, 239–247.

MARTIN, U., MÜHLE, U. & OETTEL, H. (1995). Erfahrungen mit der quantitativen Bestimmung der Versetzungsdichte im Transmissionselektronenmikroskop / The Quantitative Measurement of Dislocation Density in the Transmission Electron Microscope. *Practical Metallography* **32**, 467–477.

MAUGIS, P. & GOUNÉ, M. (2005). Kinetics of vanadium carbonitride precipitation in steel: A computer model. *Acta Materialia* **53**, 3359–3367.

MAUGIS, P. & HOUMMADA, K. (2016). A methodology for the measurement of the interfacial excess of solute at a grain boundary. *Scripta Materialia* **120**, 90–93.

MEDOUNI, I. (2022). 'Etude par sonde atomique tomographique de l'effet du vieillissement thermique dans la zone affectée thermiquement des liaisons bimétalliques des EPR'. Aix-Marseille Université https://theses.fr/2022AIXM0257 (Accessed August 28, 2023).

MEDOUNI, I., PORTAVOCE, A., MAUGIS, P., EYMEOUD, P., YESCAS, M. & HOUMMADA, K. (2021). Role of dislocation elastic field on impurity segregation in Fe-based alloys. *Scientific Reports* **11**.

MILLER, M. K. (2006). Atom probe tomography characterization of solute segregation to dislocations. *Microscopy Research and Technique* **69**, 359–365.

MOTTAY, W., HOUMMADA, K., BRÉCHET, Y., MASSARDIER, V., PERRIN-PELLEGRINO, C., MAUGIS, P., ROCH, F. & GOUNÉ, M. (2024). Identification and analysis of a reverse dynamic strain ageing in welded joints of C-Mn steels in the secondary circuit welds of nuclear power plants. *Scripta Materialia* **247**, 116099.

MOTTAY, W., MAUGIS, P., JOUIAD, M., ROCH, F., PERRIN-PELLEGRINO, C. & HOUMMADA, K. (2023). Effect of dislocation density on competitive segregation of solute atoms to dislocations. *Materials Science and Engineering: A* **881**, 145380.

PARK, H. S., KANG, J. S., YOO, J. Y. & PARK, C. G. (2010). In Situ TEM and APT Analysis on the Dislocations Associated with Solute Carbons in Strain-Aged Low Carbon Pipeline Steels. *Materials Science Forum* **654–656**, 122–125.

PASCUET, M. I., MARTÍNEZ, E., MONNET, G. & MALERBA, L. (2017). Solute effects on edge dislocation pinning in complex alpha-Fe alloys. *Journal of Nuclear Materials* **494**, 311–321.

PERELOMA, E., BATA, V. & GAZDER, A. A. (2012). The effect of chromium addition on the strain ageing and recrystallisation behaviour of low carbon steel. 12.

PERELOMA, E., BELADI, H., ZHANG, L. & TIMOKHINA, I. (2012). Understanding the Behavior of Advanced High-Strength Steels Using Atom Probe Tomography. *Metallurgical and Materials Transactions A* **43**, 3958–3971.

PERELOMA, E. & TIMOKHINA, I. (2017). Bake hardening of automotive steels. In *Automotive Steels*, pp. 259–288. Elsevier https://linkinghub.elsevier.com/retrieve/pii/B9780081006382000092 (Accessed January 6, 2022).

PERRIN TOININ, J., PORTAVOCE, A., TEXIER, M., BERTOGLIO, M. & HOUMMADA, K. (2016). Te homogeneous precipitation in Ge dislocation loop vicinity. *Applied Physics Letters* **108**, 232103.

RENDULIC, K. D. & MÜLLER, E. W. (1967). Elastic Deformation of Field-Ion-Microscope Tips. *Journal of Applied Physics* **38**, 2070–2072.

RESENDE, J., NGUYEN, V.-S., FLEISCHMANN, C., BOTTIGLIERI, L., BROCHEN, S., VANDERVORST, W., FAVRE, W., JIMÉNEZ, C., DESCHANVRES, J.-L. & NGUYEN, N. D. (2021). Grain-boundary segregation of magnesium in doped cuprous oxide and impact on electrical transport properties. *Scientific Reports* **11**, 7788.

SAKA, H. (2021). *Practical Electron Microscopy of Lattice Defects*. WORLD SCIENTIFIC https://www.worldscientific.com/worldscibooks/10.1142/12221 (Accessed October 16, 2024).

SAKSENA, A., SUN, B., DONG, X., KHANCHANDANI, H., PONGE, D. & GAULT, B. (2024). Optimizing site-specific specimen preparation for atom probe tomography by using hydrogen for visualizing radiation-induced damage. *International Journal of Hydrogen Energy* **50**, 165–174.

SMITH, G. D. W., HUDSON, D., STYMAN, P. D. & WILLIAMS, C. A. (2013). Studies of dislocations by field ion microscopy and atom probe tomography. *Philosophical Magazine* **93**, 3726–3740.

SOLIMAN, M., SHAN, Y. V., MENDEZ-MARTIN, F., KOZESCHNIK, E. & PALKOWSKI, H. (2020). Strain aging characterization and physical modelling of over-aging in dual phase steel. *Materials Science and Engineering: A* **788**, 139595.

TAKAHASHI, J., KAWAKAMI, K., HAMADA, J. & KIMURA, K. (2016). Direct observation of niobium segregation to dislocations in steel. *Acta Materialia* **107**, 415–422.

TAKAHASHI, J., KAWAKAMI, K. & KOBAYASHI, Y. (2011). Quantitative analysis of carbon content in cementite in steel by atom probe tomography. *Ultramicroscopy* **111**, 1233–1238.

TAKAHASHI, J., KAWAKAMI, K. & KOBAYASHI, Y. (2020). Study on Quantitative Analysis of Carbon and Nitrogen in Stoichiometric θ-Fe3C and γ′-Fe4N by Atom Probe Tomography. *Microscopy and Microanalysis* **26**, 185–193.

TAKAHASHI, J., KAWAKAMI, K., USHIODA, K., TAKAKI, S., NAKATA, N. & TSUCHIYAMA, T. (2012). Quantitative analysis of grain boundaries in carbon- and nitrogen-added ferritic steels by atom probe tomography. *Scripta Materialia* **66**, 207–210.

THUVANDER, M., MAGNUSSON, H. & BORGGREN, U. (2021). Carbide Precipitation in a Low Alloyed Steel during Aging Studied by Atom Probe Tomography and Thermodynamic Modeling. *Metals* **11**, 2009.

TWEDDLE, D., JOHNSON, J. A., KAPOOR, M., MILESKI, S., CARSLEY, J. E. & THOMPSON, G. B. (2022). Direct Observation of PFIB-Induced Clustering in Precipitation-Strengthened Al Alloys by Atom Probe Tomography. *Microscopy and Microanalysis* **28**, 296–301.

VEIGA, R. G. A., GOLDENSTEIN, H., PEREZ, M. & BECQUART, C. S. (2015). Monte Carlo and molecular dynamics simulations of screw dislocation locking by Cottrell atmospheres in low carbon Fe–C alloys. *Scripta Materialia* **108**, 19–22.

VEIGA, R. G. A., PEREZ, M., BECQUART, C. S. & DOMAIN, C. (2013). Atomistic modeling of carbon Cottrell atmospheres in bcc iron. *Journal of Physics: Condensed Matter* **25**, 025401.

VENTELON, L., CAILLARD, D., LÜTHI, B., CLOUET, E., RODNEY, D. & WILLAIME, F. (2023). Mobility of carbon-decorated screw dislocations in bcc iron. *Acta Materialia* **247**, 118716.

WAGNER, D., MORENO, J. C. & PRIOUL, C. (1996). Influence of Post Weld Heat Treatment on the Dynamic Strain Aging of C-Mn Steels. *Le Journal de Physique IV* **06**, C8-159-C8-162.

———— (2000). Dynamic strain ageing in C-Mn steels and associated welds. Effect of metallurgical parameters on the tensile behaviour. *Revue de Métallurgie* **97**, 1481–1500.

WILDE, J., CEREZO, A. & SMITH, G. D. W. (2000). Three-dimensional atomic-scale mapping of a cottrell atmosphere around a dislocation in iron. *Scripta Materialia* **43**, 39–48.

WILSON, D V & RUSSELL, B. (1960). The contribution of precipitation to strain ageing in low carbon steels. *Acta Metallurgica* **8**, 12.

WILSON, D.V. & RUSSELL, B. (1960). The contribution of atmosphere locking to the strain-ageing of low carbon steels. *Acta Metallurgica* **8**, 36–45.

XIAO, Y., LI, W., ZHAO, H. S., LU, X. W. & JIN, X. J. (2016). Investigation of carbon segregation during low temperature tempering in a medium carbon steel. *Materials Characterization* **117**, 84–90.

YANG, J. R. & BHADESHIA, H. K. D. H. (1990). The dislocation density of acicular ferrite in steel welds. *Welds J.* https://www.phase-trans.msm.cam.ac.uk/2002/dislocation.density.pdf (Accessed February 25, 2022).

ZANDBERGEN, M. W., XU, Q., CEREZO, A. & SMITH, G. D. W. (2015). Study of precipitation in Al–Mg–Si alloys by Atom Probe Tomography I. Microstructural changes as a function of ageing temperature. *Acta Materialia* **101**, 136–148.

ZHOU, X., MIANROODI, J. R., KWIATKOWSKI DA SILVA, A., KOENIG, T., THOMPSON, G. B., SHANTHRAJ, P., PONGE, D., GAULT, B., SVENDSEN, B. & RAABE, D. (2021). The hidden structure dependence of the chemical life of dislocations. *Science Advances* **7**, eabf0563.

ZHOU, X., YU, X., KAUB, T., MARTENS, R. L. & THOMPSON, G. B. (2016). Grain Boundary Specific Segregation in Nanocrystalline Fe(Cr). *Scientific Reports* **6**, 34642.